ALOS PALSAR and AVNIR Data for Geosciences Applications in Tropical Environments of Brazil

PI No. 219

W. R. Paradella, T. G. Rodrigues, A. R. dos Santos, C. G. de Oliveira, R. R. Marinho
National Institute for Space Research (INPE) - Remote Sensing Division (DSR)
São José dos Campos, São Paulo State - 12227-010 – BRAZIL
{waldir, athos, cleber, rogeosr}@ dsr.inpe.br, tgcart@gmail.com

ABSTRACT

This study highlighted the usage of ALOS (PALSAR, AVNIR-2) data integrated with ancillary data (SRTM-3) for cartographic and geological applications in two distinct tropical environments of Brazil: Serra dos Carajás (Pará State) and Curaçá Valley (Bahia State). A combination of altimetry derived from SRTM-3 and planimetry from PALSAR Fine Beam Dual polarization (FBD) data was evaluated aiming at producing a semi-detailed cartographic map in the mountainous area of the Serra dos Carajás, Amazon region. The quality of the orbital topographic information was evaluated regarding precise planialtimetric measurements acquired from Global Positioning System (GPS) field campaigns. The evaluations were performed following two approaches: (1) the use of Root Mean Square Error (RMSE) and (2) calculations of tendency and precision analysis. The investigation has shown that the planialtimetric quality of the orbital products fulfilled the Brazilian Map Accuracy Standards requirements for 1:100,000 A Class map. In the semi-arid terrain of the Curaçá Valley, the value of digital integration of PALSAR Fine Beam Single polarization (FBS), Polarimetric Mode (PLR) and Advanced Visible and Near-Infrared Radiometer (AVNIR-2) data, calibrated with field information, was evaluated for structural geological mapping. Special emphasis was placed on the use of IHS (FBS/PLR) and arithmetical (FBS/AVNIR-2) schemes for the production of value-added integrated products. The investigation with ALOS data allowed the re-evaluation of previous geological information and the precise characterization of distinct structural domains in the area.

1. INTRODUCTION

The Brazilian Amazon is a vast territory (almost 5.5 million km^2) with an enormous need for mapping and monitoring of renewable and non-renewable resources. Almost 35% of the region is without semi-detailed planialtimetric information, corresponding to 616 topographic sheets in the 1:100,000 scale [1]. In addition, the available information for the remainder of the region was mainly produced in the time-frame of 1960 and 1980, and needs to be up-dated or re-mapped. The usage of optical images for basis coverage is expensive or even not possible due to adverse atmospheric conditions. With the SRTM mission in February 2000, interferometric DEMs were available as a free access data for the globe [2]. First evaluation of the altimetric quality from SRTM-3 (3-arc seconds by 3-arc seconds), in flat and mountainous relief of Brazilian Amazon, has indicated a RMSE of 12 m in elevation that fulfilled the topographic mapping requirements for 1:100,000 A Class [3]. These findings justified the choice of SRTM-3 data as a primary elevation source for semi-detailed topographic mapping in the region. However, it is important to mention that for cartographic production up-dated planimetric information is also necessary. The classification of topographic maps in Brazil should be performed in accordance to the National Cartographic Accuracy Standard (PEC in Portuguese), established by the Brazilian Cartographic Commission. PEC is a statistical indicator (90% of probability) for planialtimetric accuracy, corresponding to 1.6449 times the RMSE (PEC = 1.6449 × RMSE). For a 1:100,000 scale A Class map, the altimetric and planimetric PEC limits are 25 m (RMSE = 16.66 m) and 50 m (RMSE = 30 m), respectively. The advent of the ALOS satellite in January 2006, with an L-band SAR sensor, opened new perspectives to a wide range of applications in the Geosciences. PALSAR imageries with distinct attributes of high-resolution, variable incidence, multi-polarization and polarimetric capabilities have been collected under the ALOS RA # 219 in the Serra dos Carajás, Brazilian Amazon. In this research, we expanded the previous research with PALSAR data in the region [4]. Now, we have analyzed the feasibility of using planialtimetric and thematic information from FBD ortho-images integrated with altimetric information from SRTM-3 to produce a topographic map, which met the requirements for 1: 100,000 (A Class) as requested by the Brazilian Standard for Cartographic Accuracy. On the other hand, a set of FBS, PLR and AVNIR-2 data was also acquired in Curaçá Valley, a representative terrain of the tropical semi-arid environment of Brazil. In this area, precipitation is generally concentrated over a short period of time and irregularly distributed over small sectors. Residual soils, presence of outcrops and moderate to low-density Caatinga vegetation favor a geologic SAR investigation since it is often difficult to make a direct relationship between rock alteration products with SAR responses. Thus, value-added PALSAR-AVNIR-2 products were photogeologically interpreted in the enhancement of structures and erosional surface features, closely related to bedrock and structural variations with tectonic implications in the area.

2.2. SERRA DOS CARAJÁS INVESTIGATION

The Serra dos Carajás is located on the easternmost border of the Amazon Region including Água Azul do Norte, Canaã dos Carajás, Curionópolis, Marabá and Parauapebas municipalities (figure 1). The region is characterized by a set of hills and plateaus (altitudes from 500 to 900 meters) surrounded by southern and northern lowlands (altitudes around 200 meters), totally covered by Ombrophilous Equatorial forest.

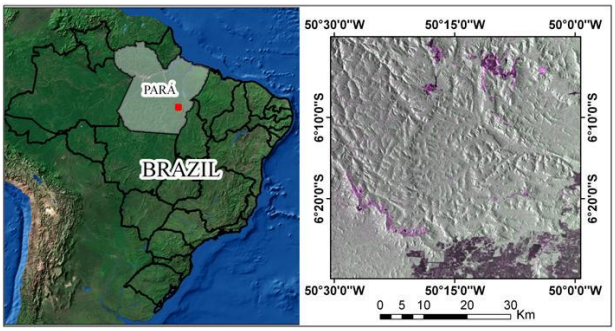

Figure 1. Location of the Serra dos Carajás.

The study site comprises around 3,059.47 km^2 corresponding to the Serra dos Carajás (SB-22-Z-A-II) 1:100,000 scale topographic sheet, which was produced from airphotos by IBGE (Brazilian Institute of Geography and Statistics) during the 1967-1981 period. Chemical weathering, thick oxisols ("latosols"), few outcrops and thick tropical rainforest are some of the main characteristics of the region. The area is within the Carajás Mineral Province, the most important Brazilian mineral province with world's largest iron deposits and important deposits of Mn (Azul), Cu (Salobo, Sossego), Ni (Vermelho), among others. Due to the economic importance of this area there is an increasing need to provide accurate maps to support exploration and also environmental programs. A reasonable amount of optical and radar data has been acquired and evaluated for geological and topographic mapping in this region [5], [6], [7], [8], [9].

2.1. DATASET

PALSAR imageries available for this investigation were acquired over the test site through two passes in September 2007. A total of four FBD scenes (L-HH, L-HV polarizations) was collected under distinct look-azimuth (descending pass-west looking, ascending pass-east looking), moderate incidence, and a swath width of 75 km (table I).

Table 1. FBD data

Image Id	080153740	080153750	076437060	076437050
Product Level	1.5	1.5	1.5	1.5
Polarization	HH, HV	HH, HV	HH, HV	HH, HV
Look Azimuth	282° (desc.)	282° (desc.)	78° (asc.)	78° (asc.)
Acquisition	27/Sept/07	27/Sept/07	27/Sept/07	27/Sept/07
Incidence	38.894°	38.894°	39.019°	39.019°
Looks (rg x az)	4 × 1	4 × 1	4 × 1	4 × 1
Resolution rg × az (m)	9.6 × 4.49	9.6 × 4.49	9.6 × 4.49	9.6 × 4.49

On February 11, 2000, the SRTM payload onboard Space Shuttle Endeavour was launched into space to acquire topographic (elevation) data. A C-band DEM related to the test-site was originally produced with 1-second original data (30 m of spatial resolution) and further was downgraded to a resolution of 3 arc-seconds or 90 m of spatial resolution (SRTM-3). This data was acquired at ftp://e0srp01u.ecs.nasa.gov/srtm/version2/SRTM3 in Lat/Long coordinates related to the World Geodetic System 1984 (WGS84) ellipsoid and the Earth Gravitational Model 1996 (EGM96) vertical datum and available in HGT file format. In addition, precise planialtimetric measurements from Global Positioning System (GPS) were acquired in the test-site and used as Ground Control Points (GCPs) for the ortho-rectification of the FBD images and as Independent Check Points (ICPs) for calculation of altimetric (SRTM-3) and planimetric (FBD images) accuracies. Two dual frequency Geodetic GPS receptors were used for the static GPS measurements and a total of 48 static measurements and 35,000 kinematics measurements were collected during field campaigns in September-October 2002 using helicopter and vehicle. The maximum errors with a probability of 68.3% (1 σ) for the estimated positions were 18 cm (latitude), 75 cm (longitude) and 24 cm (ellipsoidal height) in geodetic coordinates related to the WGS84 ellipsoid.

2.2. METHODOLOGICAL APPROACH

2.2.1. PROCESSING OF SRTM-3 DEM

The SRTM-3 DEMs data were imported and merged into a continuous PCI Geomatica file format (PIX), with 90 m pixel spacing, followed by the application of an interpolation function to fill no-data holes based on Geomatica Focus from PCI software [10]. In order to become compatible the SRTM-3 DEM and GPS points datum with the reference datum adopted in Brazil (SAD69/Imbituba), the following steps were necessary: (a) SRTM-3 DEM - calculation of the geoid undulation of the EGM96 model using the INPT software from NGA [11]; (b) SRTM-3 DEM - conversion of the orthometric altitude (EGM96) to ellipsoidal altitude (WGS84); (c) SRTM-3 DEM and GPS measurements - calculation of the geoid undulation for the orthometric altitude determination (Imbituba) using MAPGEO 2004 software [12]; (d) SRTM-3 DEM and GPS measurements - conversion of the ellipsoidal altitude (WGS84) to orthometric altitude (Imbituba) and (e) SRTM-3 DEM and GPS measurements - conversion data from WGS84 to SAD69 using PCI Geomatica software. Finally, a contour lines vector segment was produced with 50 meter interval from the raster SRTM-3 DEM (UTM projection, SAD69 and Imbituba vertical datum).

2.2.2. FBD DATA ORTHO-RECTIFICATION

Since the test-area has significant topographic relief, the geometric correction should take this into consideration. The geometric correction was based on a mathematical and accurate geometric model (ortho-rectification), which considers the distinct distortions relative to the global

geometry of viewing, such as distortions relative to the platform, to the sensor, Earth geoid-ellipsoid including elevation, and cartographic projection (ellipsoid-cartographic plane). This adapted model (Toutin's 3D Radargrammetric) represents the well-known collinearity condition (and coplanarity condition for stereo model), and integrates the different distortions relative to the global geometry of view, including effects relative to the platform, to the sensor, to the Earth and to the cartographic projection. This model is embodied into PCI Geomatica OrthoEngine software and the techniques implemented in this software are presented in [13]. FBD images were ortho-rectified using Toutin's 3D Radargrammetric with 28 GCPs and the SRTM-3 DEM. The Enhanced Frost Filter (3 × 3 pixels window) was used to filter the speckle noise. Finally, with the geometrically correct images it was produced two mosaics, one with ascending and the other with the descending scenes.

2.2.3. STATISTICAL ANALYSIS

The altimetric accuracy of the SRTM-3 DEM was estimated by comparison of the DEM elevation values (Z_i) and the real values given by ICPs (Z_{GPS}). For the planimetric evaluation of the PALSAR mosaics, the comparison was between planimetric coordinates (E_i, N_i) of the products and the planimetrics values from ICPs (E_{GPS}, N_{GPS}). The accuracy analysis was carried out following two approaches: (a) the overall classifications of the SRTM-3 DEM considering the altimetric PEC, and of the DEM and FBD mosaics regarding the planimetric PEC, and (b) calculations of tendency and precision analysis for both data. The altimetric quality of the SRTM-3 DEM was estimated based on $RMSE_A$ values given by the Equation 1 ([14], [15]), and on VMAS (Vertical Map Accuracy Standard) values, which correspond to the vertical error with 90% of probability (Equation 2, [15]).

$$RMSE_A = \sqrt{\sum(Z_i - Z_{GPS})^2/n} \quad (1)$$

$$VMAS = 1.6449 \times RMS_A \quad (2)$$

where n is the number of sample points.

For the planimetric classification of the DEM and the FBD mosaics, planimetric $RMSE_A$ (Equation 3, [14], [15]) and CMAS (Circular Map Accuracy Standard) values, which represent the circular error with 90% de probabilities (Equation 4) were also used.

$$RMSE_P = \sqrt{\sum(E_i - E_{GPS})^2 + (N_i - N_{GPS})^2/n} \quad (3)$$

$$CMAS = 2.146 \times RMSE_P \quad (4)$$

where n is the number of sample points. Finally, the calculations of tendency and precision analysis were based on the methodology proposed by [16], which takes into account computed discrepancies and standard deviations. Tendency analysis was used to check the presence of systematic errors. It was based on the hypothesis ($H_0: \hat{\mu} = 0$; $H_1: \hat{\mu} \neq 0$) whose acceptance or rejection is controlled by the computed Student t statistics test (Equation 5) compared with the theoretical $t_{(n-1,\alpha/2)}$ value.

$$t_x = \frac{\hat{\mu}}{\hat{\sigma}} \times \sqrt{n} \quad (5)$$

where n is the number of sample points. Precision analysis uses comparison of the variance of sample deviations ($\hat{\sigma}^2$) to their respective pre-defined (tabled) values. The test is carried out using a hypothesis about the mean and standard deviation of the sample for each of the altimetric value. *Chi-squared* (χ^2) is the statistical test that was applied. The accuracy was estimated in the Z values using standard statistical methodology involving the comparison of a sample value of χ^2 and the tabled value $\chi^2_{(n-1,\alpha)}$. This analysis will point out if the product fulfills the accuracy for the requested scale.

$$\chi^2_x = (n-1) \times \hat{\sigma}^2 / \widehat{\sigma}^2_x \quad (6)$$

where n is the number of sample points.

2.3. RESULTS AND DISCUSSION

A total of 30 ICPs was selected for the planialtimetric evaluation of the SRTM-3 DEM (figure 2). For the ortho-rectification process of the FBD scenes, 28 GCPs were used for the modeling and ortho-images generation and 32 ICPs for the planimetric quality assessment (figure 3). The quantitative results for the SRTM-3 DEM are presented in Table 2. The analysis of these results allows important findings: (1) using the PEC classification limit and the results of Chi-squared the SRTM-3 DEM altimetry fulfilled the requirements for a 1:100,000 scale A Class map; (2) however, the statistics of tendency analysis indicated the presence of a positive offset in the Z direction.

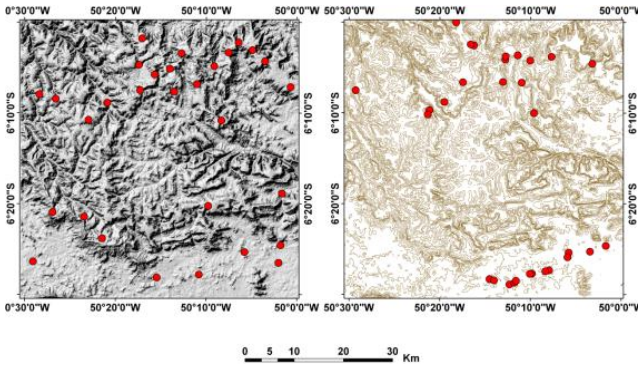

Figure 2. Distribution of the ICPs for the altimetric and planimetric evaluation of the SRTM-3 DEM.

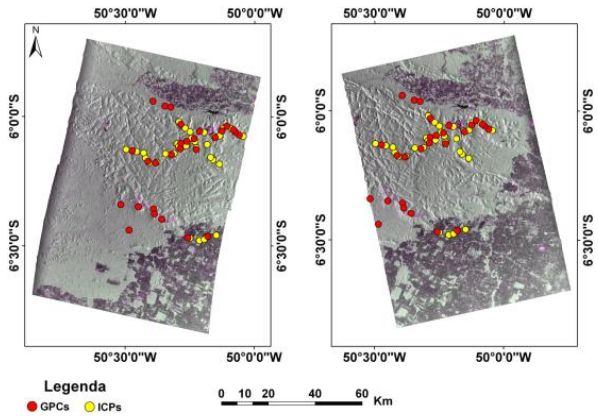

Figure 3. GCPs (yellow dots) and ICPs (red dots) distribution of the for the descending and ascending FBD mosaics.

Table 2. Values of Mean of Discrepancy, Standard Deviation, RMSE, VMAS, Tendency and Precision analysis of SRTM-3 DEM.

$\hat{\mu}_Z\ (m)$	7.977
$\hat{\sigma}_Z\ (m)$	5.441
$RMSE_z\ (m)$	9.605
$VMAS_z\ (m)$	15.798
$t_{(n-1;\,5\%)}$	1.699
$t_{Z(sample)}$	8.029
$\chi^2{}_{(n-1;10\%)}$	39.087
$\chi^2{}_{Z(sample)}$	3,091
$\lvert t_{Z(sample)}\rvert < t_{(n-1;\,5\%)}$	False
$\chi^2{}_{Z(sample)} < \chi^2{}_{(n-1;10\%)}$	True

Regarding the planimetric assessment of SRTM3 and FBD-mosaics, the results are presented in table 3. These results show that the planimetric accuracy of SRTM-3 DEM and FBD mosaics (RMSE $\leq$ 21,21 m) also fulfilled the PEC requirements for 1: 100,000 A Class Map. In addition, no bias detected for the interferometric DEM, while a systematic offset (bias) in planimetry is present for the N component in the FBD mosaics. Usually, elevation information is expressed in cartographic maps by contour lines. The results confirmed the altimetric and planimetric quality of contour lines produced from SRTM-3 DEM and highlighted its potential as input for cartographic map production at semi-detailed scale. On the other hand, due to the ability of FDB PALSAR imagery to highlight target variations on the terrain, distinct image patterns with arrays of tonal/textural patterns can be meaningfully related to important layers (drainages, roads, land-use, etc.), which are also necessary as thematic information for mapping purposes. Figure 4 shows an example of the combination of information from SRTM-3 DEM (contour lines) and FBD PALSAR (drainage, land-use and vegetation patterns) for cartographic applications that fulfilled planialtimetric PEC limits for1:100,000 A Class. More details of this investigation in Carajás can be found in [17].

3. THE CURAÇÁ VALLEY INVESTIGATION

The Curaçá Valley is part of a Cu-rich province located on the Bahia State (figure 5). The climate in the region is tropical semiarid, with average temperature around 30° C and between 300 and 700 mm of annual rainfall, which occurs in the Summer (January to March) marked by heavy showers of short duration. At such times, normally dry valleys become fast-flowing streams and flooding occurs on the low flat lands. Topographically, the area is characterized by a land surface eroded to a nearly flat plain, with altitudes ranging from 330 to 830 m above sea level. In this pediplain, the altimetric variation among watersheds is approximately 20 m. Soils are generally shallow (30 cm to 1.5 m) but relatively fertile, except for the organic matter content.

Table 3. Values of Discrepancy Mean ($\hat{\mu}$), Standard Deviation ($\hat{\sigma}$), Root Mean Square Error ($RMSE_P$), Vertical Map Accuracy Standard (VMAS), Tendency and Precision analysis of SRTM-3 and PALSAR planimetry.

	SRTM-3	Descending FBD Mosaic	Ascending FBD Mosaic
$\hat{\mu}_E$ (m)	2.096	1.045	-0.224
$\hat{\sigma}_E$ (m)	16.197	8.715	5.620
$RMSE_E$ (m)	16.062	8.641	5.537
$CMAS_E$ (m)	34.468	18.508	11.857
$t_{(n-1;\,5\%)}$	1.699	1.695	1.695
$t_{E(sample)}$	0.709	0.678	-0.2414
$\chi^2{}_{(n-1;10\%)}$	39.087	41.422	41.422
$\chi^2{}_{E(sample)}$	16.906	5.233	2.176
$\lvert t_{E(sample)}\rvert < t_{(n-1;\,5\%)}$	True	True	True
$\chi^2{}_{E(sample)} < \chi^2{}_{(n-1;10\%)}$	True	True	True
$\hat{\mu}_N$ (m)	-0.575	5.762	3.035
$\hat{\sigma}_N$ (m)	11.611	9.531	6.577
$RMSE_N$ (m)	11.431	11.010	7.150
$CMAS_N$ (m)	24.530	23.578	15.312
$t_{(n-1;\,5\%)}$	1.699	1.695	1.695
$t_{N(sample)}$	-0.271	3.420	2.610
$\chi^2{}_{(n-1;10\%)}$	39.087	41.422	41.422
$\chi^2{}_{N(sample)}$	8.689	6.258	2.980
$\lvert t_{N(sample)}\rvert < t_{(n-1;\,5\%)}$	True	False	False
$\chi^2{}_{N(sample)} < \chi^2{}_{(n-1;10\%)}$	True	True	True

Conversely, drainage channels work as accumulation sites and tend to have deep deposits that receive a large volume of transported and partly weathered material, mainly rock fragments. Annual fluctuations in climatic conditions, especially rainfall, have resulted in variations in the Caatinga vegetation physiognomy and phenology, but dominant in the area are deciduous woody shrubs (4 to 7 m in height), with variable cover density, canopy structure and stratification (up to three strata)

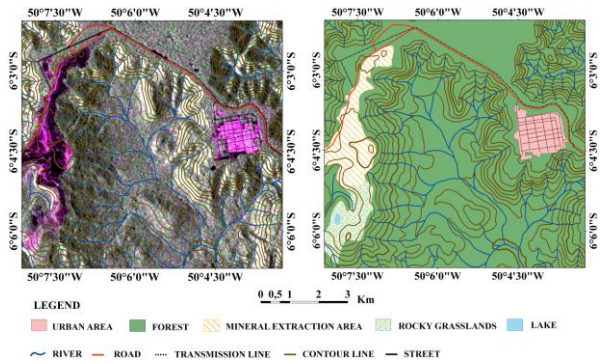

Figure 4. Example of the combination of information from SRTM-3 DEM (contour lines) and FBD PALSAR (drainage, land-use and vegetation patterns).

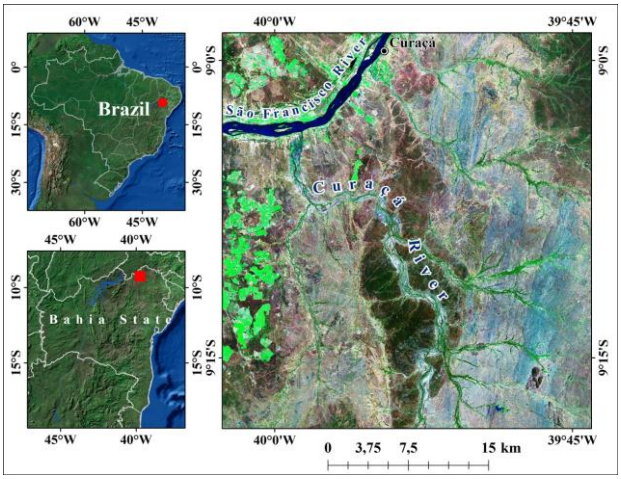

Figure 5. Location of the Curaçá River Valley

The deciduous perennials shed their leaves in May or earlier and are dormant up to the beginning of the rainy season, around December. This xerophytic vegetation and very shallow residual soils allowed rock discrimination based on optical and SAR data [18], [19]. Geological, geochronological and isotopic research have identified four important Archean crustal segments in the basement of the São Francisco Craton in the State of Bahia [20]. During the Paleoproterozoic Transamazonian Orogeny (2.0 Ga.), a NW–SE oriented collision of the four blocks took place and has resulted in the reorientation of the main structural and lithological units towards NS with strong E-W crustal shortening and sinistral kinematics (figure 6). This event has resulted in the formation of the Itabuna-Salvador-Curaçá (ISC) belt, where the test-area is inserted. The lithological units in the region can be grouped as Archean gneisses and granulites interbedded quartzites, amphibolites, mafic-ultramafic intrusives and Upper Proterozoic marbles/limestones, schists, and phyllites [21]. The gneissic-granulitic complex is cut by Cu-mineralized intrusives with reserves exceeding 150 million tonnes of ore (0.5 to 1.0% average Cu grade). Massive sulfides are associated with pyroxenites and weak disseminated sulfides to norites, gabbro-norites and anorthosites.

3.1. ALOS DATASET

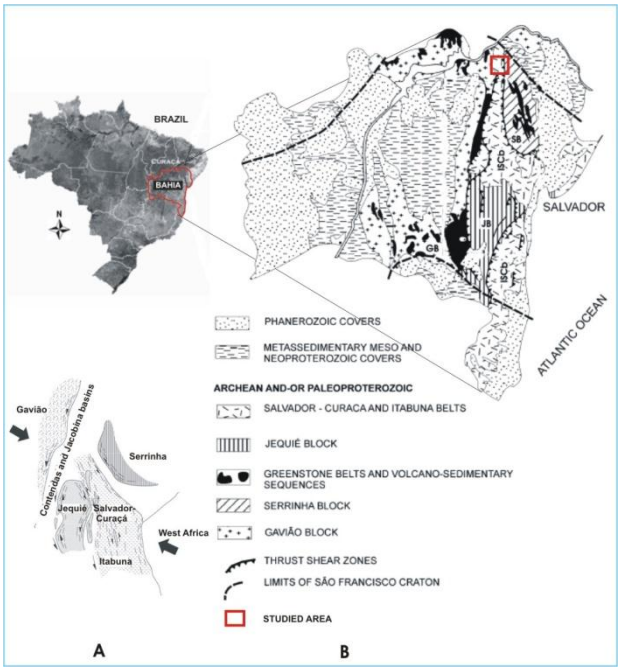

Figure 6. Evolution of the São Francisco Craton in the Bahia state showing the situation of the Archean blocks before (a) and after (b) the Paleoproterozoic collision [20].

Three distinct ALOS dataset were explored in this investigation:FBS, PLR and AVNIR-2 data (details of the images are seen in tables 4 and 5). The images were acquired during the dry (AVNIR-2 and FBS) and wet (PLR) seasons in the region.

Table 4. AVNIR-2 data

Scene Id	ALAV2A204723780
Sun Elevationn	68°
Sun Azimuth	125°
Acquisition Date	2009/Nov/27
Incidence	38.894°
Spatial Resolution (m)	10

Table 5. FBS and PLR data

Scene id	FBS: ALPSRP 081753800	FBS: ALPSR 081753810	PLR: ALPSRP 169497010
Product Level	1.5	1.5	1.1
Polarization	HH	HH	HH, HV, VH, VV
Orbit	Descending	Descending	Ascending
Acquisition Date	2007/Aug/07	2007/Aug/07	2009/Mar/31
Incidence	38°	38°	24.3°
Looks rg x az	1 x 2	1 x 2	1 x1
Spatial Resolution rg x az (m)	4.7 x 4.49	4.7 x 4.49	4.7 x 4.49
Pixel Spacing (m	6.5 x 6.5	6.5 x 6.5	6.5 x 6.5

3.2. METHODOLOGICAL APPROACH

AVNIR-2 images were orthorectified based on Toutin´s modeling [8] and using as input planialtimetric information from 15 field GCPs and SRTM-3 DEM (RMS error values were X = 1.88m and Y = 1.97m). PALSAR images were radiometrically (Kuan and Lee speckle filtering) and geometrically corrected. The FBS image was orthorectifed through the use of the Radar Specific package [10] taking into account the available ephemerides information at the scene metadata (total RMS error of 3.53 m). The PLR data were converted from SLC to covariance matrix [C], speckle filtered (Lee polarimetric filter) and extracted the intensity channels, which were orthorectified through the use of Rational Functions [10] and 9 GCPs (RMS error values were X = 11.57 m and Y= 13.11m). Finally, taking into account the statistics of geometric correction and in order to keep a balance of the geometric and the radiometric integrity in the final integration, a 10 m pixel size was chosen as a common pixel size for the data integration. The SAR images were digital enhanced by linear contrast-stretch, and colors were assigned to the PLR intensity multipolarized channels. In addition, digital integrations (fusion) of FBS with PLR through IHS transform and FBS with AVNIR-2 based on arithmetic (multiplication) schemes were carried out aiming at producing distinct value-added products that facilitated the extraction of geological information. The visual interpretation of the integrated products was based on the scheme proposed by [22] and consisted in the analysis of linear features with geological-structural significance given by drainage and relief elements. For the drainage, the following elements were considered: frequency of textural elements (related to rock types), symmetric-asymmetric patterns (attitude of planar structures), linear features (foliations, fractures, bedding) and array (kinematic and complexity of structures). For the relief, the elements were considered as follows: frequency of textural elements (rock types), symmetric-asymmetric patterns (attitude of planar structures), negative ruptures (lithological contacts), positive linear features (faults, dikes, etc.) and array (kinematic and/or complexity of structures). In addition, spectral attributes in the colour composites were also considered, which were provided by the contribution of the multipolarized PLR (HH, HV, VV) and multispectral AVNIR-2 images.

3.3. RESULTS AND DISCUSSIONS

Previous studies with airborne and orbital SAR data in the region ([23], [24]) have reported the presence of two distinct orientation systems of linear features related to metamorphic foliations: N10°-20°E, the most prominent trend, and N20°-30°E set, a secondary system restricted to eastern sector of the valley. This second system seems to define an important lithostructural limit that is associated with two contrasting metamorphic terrains from west to east across the region: migmatitic rocks (western sector) and granulitic associations (eastern sector). The IHS integration of PLR and FBS data (left) and the corresponding geological map[23] are seen in figure 6. Three intensity PLR channels (HH,HV,VV) were used as input bands in the RGB/IHS transform (hexacone model) for the hue and saturation modulations. FBS channel was linearly stretched and further used as the intensity channel in the reverse IHS-RGB transformation. The use of FBS as intensity in the digital integration has two advantages for structural mapping in the region: a better spatial resolution for the detection of minor expression of structures and the favorable look-direction (descending orbit) almost orthogonal to the structures striking NNE that are enhanced. The integrated product was visually interpreted from a regional perspective and a sub-sector was selected for a detailed analysis. In this sector (Figure 7), it was examined the lithostructural relationships between the basement rocks (migmatite, biotite-hornblende gneiss, quatz-gneiss and biotite-hypersthene gneiss) and regional geological structures, within the evolutional context of Paleoproterozoic collision (limits of Serrinha block and ISC belt).

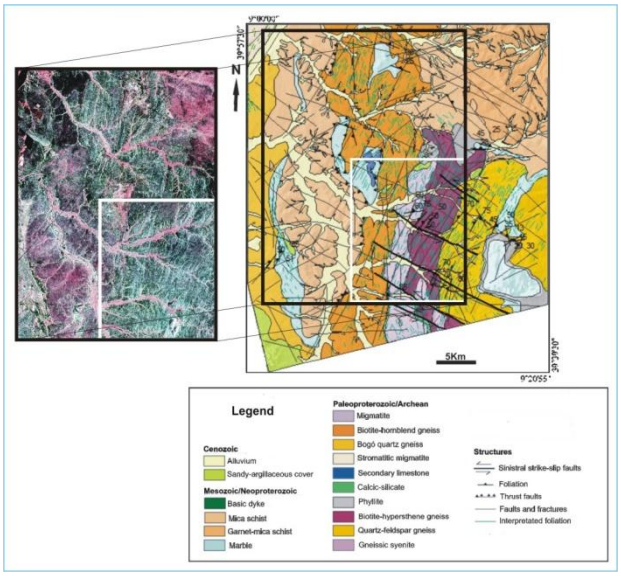

Figure 7. PLR-FBS Integration based on IHS (left) and corresponding geological map (right). Geology are in accordance to [23]. The location of the study area is outlined (white).

Distinct schemes (multipolarized color composites, IHS and multiplication) for the integration of PALSAR and AVNIR-2 data were assessed. Well-defined linear (drainage-relief) features related to the topographic breaks are indicators of foliation systems and are clearly detected in the enhanced products (figure 8). In all the integrated products, it is evident a lithostructural control marked by the two foliation systems (N20°-30° and N10°-20°E) and a lithological limit involving migmatitic and biotite-hypersthene gneissic units.. To assess the relationships between structures extracted from the images and bedrock structures/lithologies, a field campaign with detailed structural mapping was carried in the area. The structural measurements indicated that the rocks are affected by ductile deformation forming two steeply dipping foliation systems with a difference around 20° in orientation. In addition, the N20°-30° subvertical gneissic system presents a terminal asymptotic curvature towards the lithostructural limit, which characterizes a kinematic indicator of a sinistral deformation event along the N10°-20° foliation of the migmatites. This kinematic is in accordance to the proposed scheme of Paleoproterozoic Serrinha-ISC collision, which resulted on regional NS trending structures and sinistral movements (Figure 9). In

conclusion, the integration of PALSAR (FBD, PLR) and AVNIR-2 images has provided valuable textural information with structural meaning that can be used for improving the geological knowledge of the lower Curaçá Valley. The interpretation map has allowed a refinement of existing 1: 50,000 geological map particularly the accurate delimitation of this lithostructural boundary with relevant tectonic meaning.

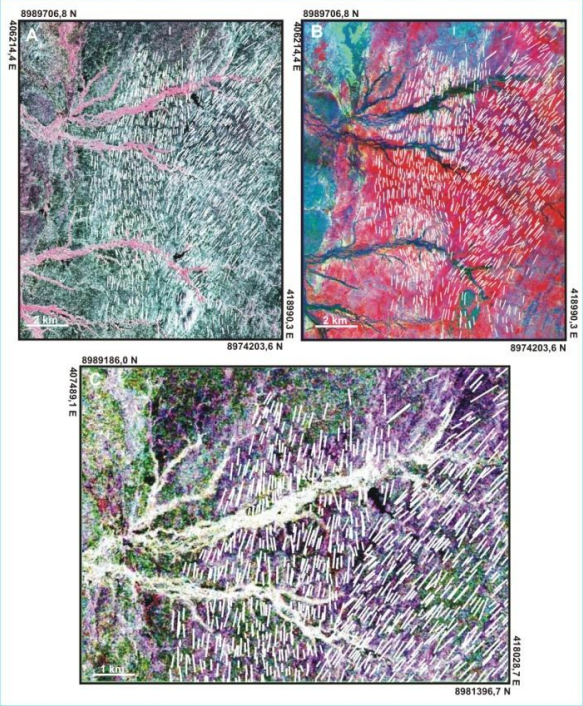

Figure 8. Examples of integration: RGB PLR (HH, HV, VV), Multiplication (FBS vs. AVNIR-2 B4, B3, B2), IHS (PLR-FBS) and interpreted foliation systems.

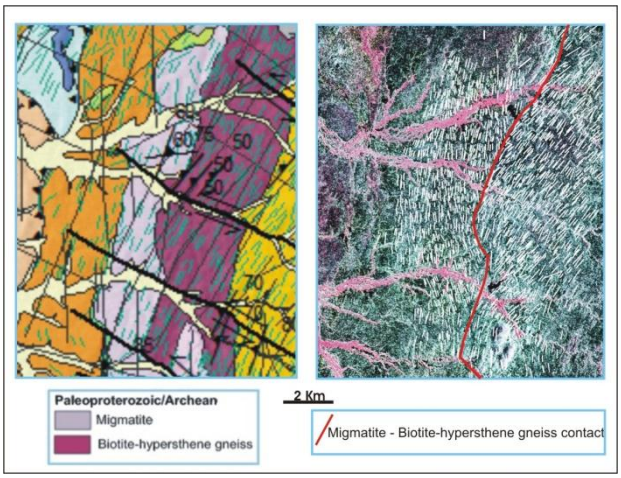

Figure 8. Geological map [15] and corresponding area with interpretation of foliation systems from the IHS integration (PALSAR-FBS).

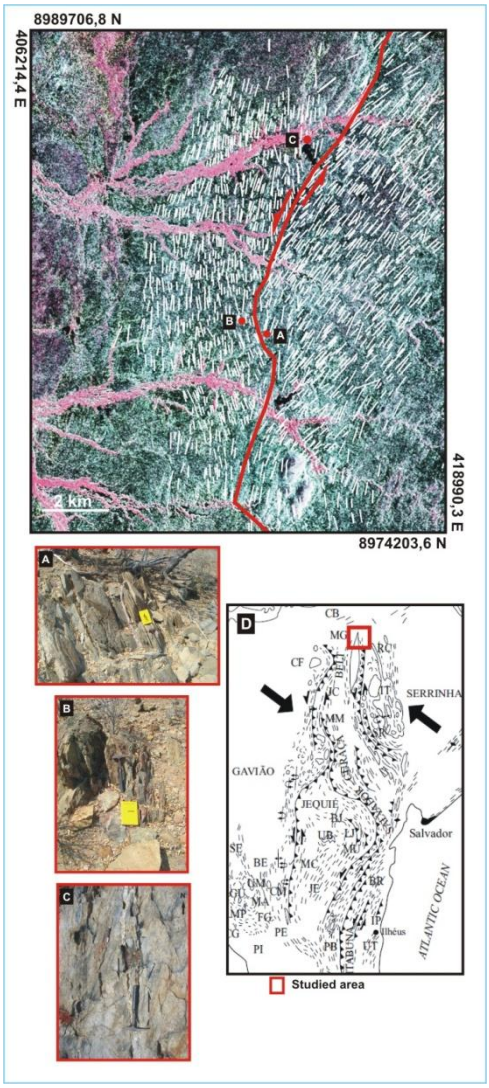

Figure 9. IHS integration of FBS-PLR showing kinematic indicator of a sinistral shear zone of strike-slip type, with small oblique movement from the secondary N20°-30° foliation against the N10°-20° main system. Legend: (a) outcrop of migmatitic rock with trending N10°E subvertical foliation, (b) outcrop of biotite-hypersthene gneiss with trending N30°E subvertical foliation, (c) Evidence of a ductile sinistral kinematic indicator given by the drag movement of N30°E/subvert secondary foliation along the regional trending N10°E/subvertical foliation; (d) tectonic model showing the proposed Archean blocks after the Paleoproterozoic collision [20].

4. ACKNOWLEDGEMNTS

This research was conducted under the agreement of JAXA Research Announcement (RA # 219). Special thanks to CNPq for the first author's grant (Process 304254/2009-6).

5. REFERENCES

[1] (SBC) Sociedade Brasileira de Cartografia. 2006. Sociedade Brasileira de Cartografia. Contribuição do Exercito à questão Amazônica - A questão do vazio Cartográfico. Boletim – Trimestral Janeiro/ Fevereiro/ Março n. 62.

[2] Farr T.G; Rosen P.A.; Caro E.; Crippen R.; Duren R.; Hensley S.; Kobrick M.; Paller M.; Rodrigues E.; Roth L.; Seal D.; Shaffer S.; Shimada J.; Umland J.; Werner M.; Oskin M.; Burbank D.; Alsdorf D. 2007. The Shuttle Radar Topography Mission. Reviews of Geophysics, 45, RG2004, doi:10.1029/2005RG000183.

[3] Oliveira C.G.; Paradella W.R. 2008. An Assessment of the Altimetric Information Derived from Spaceborne SAR (RADARSAT-1, SRTM3) and Optical (ASTER) Data for Cartographic Application in the Amazon Region. *Sensors*, 8: 3819–3829.

[4] Silva A.Q.; Paradella W.R.; Freitas C.C.; Oliveira C.G. 2009. Relationship Between PALSAR Backscatter and Surface-Roughness Parametrs from Iron Laterites in Carajás, Amazon Region. *IEEE Transactions on Geoscience and Remote Sensing*, 47 (12): 4027-4031.

[5] Paradella W.R.; Veneziani P.; Bignelli P.A.; Pietsch R. W.; Toutin T. 1997. Airborne and spaceborne synthetic aperture radar (SAR) integration with Landsat TM and gamma ray spectrometry for geological mapping in a tropical rainforest environment, the Carajás mineral province, Brazil. *International Journal of Remote Sensing*, 18 (7): 1483-1501.

[6] Paradella W.R.; Oliveira C.G.; Cecarelli I.C.F.; Cottini C.P.; Okida R. 2005. Operational Use of RADARSAT-1 Fine Stereoscopy Integrated with TM-Landsat 5 Data for Cartographic Application in the Brazilian Amazon. *Canadian Journal of Remote Sensing*, 31 (2):139-148.

[7] Teruiya R.K.; Paradella W.R.; Santos A.R.; Dall'Agnol R.; Veneziani P. 2008. Integrating airborne SAR, Landsat TM and airborne geophysics data for improving geological mapping in the Amazon region: the Cigano Granite, Carajás Province, Brazil. *International Journal of Remote Sensing*, 29 (13): 3957-3974.

[8] Oliveira C.G.; Paradella W.R. 2009. Evaluating the quality of the Digital Elevation Models produced from ASTER stereoscopy for topographic mapping in the Brazilian Amazon Region. *Annals of the Brazilian Academy of Sciences*, 81 (2): 217-225.

[9] Oliveira C.G.; Paradella W.R.; Silva A. Q. 2011. Assessment of radargrammetric DSMs from TerraSAR-X Stripmap images in a mountainous relief area of the Amazon region. *ISPRS Journal of Photogrammetry and Remote Sensing*, 66(1): 67-72.

[10] PCI Geomatics. 2010. Geomatica OrthoEngine User Guide, version 10.3, Richmond Hill, Canada: 179 p.

[11] NGA (NATIONAL GEOSPATIAL-INTELLIGENCE AGENCY) 2009. USA. Information about WGS84, EGM96.

[12] IBGE (Instituto Brasileiro de Geografia e Estatística). 2009. MAPGEO – Modelo de Ondulação Geoidal, Rio de Janeiro, Brazil

[13] Ostrowski, J.A.; Cheng, P. 2000. DEM extraction from stereo SAR satellite imagery. In: IGARSS'00: Proceedings of the International Geoscience and Remote Sensing Symposium, 25–28 July 2000, Honolulu, Hawaii. T.I. Stein. IEEE, New York.

[14] ASPRS (American Society for Photogrammetry and Remote Sensing) 1989. ASPRS Interim Accuracy Stardars for Large-Scale Maps. *Photogrammetric Engineering & Remote Sensing* 1038–1040.

[15] NSDI (National Spatial Data Infrastructure) 1998. Geospatial Positioning Accuracy Standards Part 3: National Standard for Spatial Data Accuracy. Disponível em: < http://www.fgdc.gov/standards/projects/FGDC-standards-projects/accuracy/part3/chapter3>. Acessed in: 10/09/2009.

[16] Galo M.; Camargo P.O. 1994. O uso do GPS no controle de qualidade de cartas. In.: Congresso Brasileiro de Cadastro Técnico Multifinalitário (COBRAC-1994), 1, 1994, Florianópolis, SC. Annals... Florianópolis: UFSC.

[17] Rodrigues T. G.; Paradella W. R.; Oliveira C. G. 2011. Evaluation of the altimetry from SRTM-3 and planimetry from high-resolution PALSAR FBD data for semi-detailed topographic mapping in the Amazon Region. *Annals of the Brazilian Academy of Sciences* (in press).

[18] Paradella, W. R.;Vitorello, I. 1995. Geobotanical and Soil Spectral Investigation for Rock Discrimination in the "Caatinga" Environment Based on Multitemporal Remote Sensing Data. *Canadian Journal of Remote Sensing*, 21 (1): 52-59.

[19] Paradella W.R.;Silva A.Q.; Knust S.S.A.; Rabelo T.N.; Santos A.R.; Rennó C.D.; Oliveira C.G.; Rodrigues T.G. 2009. Effect of Microtopography on RADARSAT-1 and PALSAR Backscattering from Rock Alteration Products in the Curaçá Valley. *Canadian Journal of Remote Sensing*, 35 (3): 262-269.

[20] Barbosa, J.S.F.; Sabaté, P. 2002. Geological features and the Paleoproterozoic collision of four Archean crustal segments of the São Francisco Craton, Bahia, Brazil: A synthesis. *Annals of the Brazilian Academy of Sciences*,74(2): 343-359.

[21] Delgado I.M.; Souza J.D. 1974. Curaçá-Copper Project: Economic Geology of the Copper District of Curaçá River, Bahia,Brazil. Brazilian Geological Survey (CPRM), Salvador, Brazil, 3 vols.

[22] Santos, A.R.; Veneziani, P.; Paradella, W.R.; Morais, M.C. 2001. Radar aplicado ao mapeamento geológico e prospeçcão mineral: aplicações. Curso INPE/ADIMB, 21-26 August 2000. São José dos Campos, 103 pp. (INPE-8117-PUD/45).

[23] Knust S.S.A. 2007. Avaliação das imagens RADARSAT-1 sob diferentes geometrias de observação em aplicação geológica no Vale do Rio Curaçá (Bahia). M.Sc. thesis in Remote Sensing, INPE.

[24] Rabelo, T.N.; Paradella W. R ; Santos, A. R ; Knust, S.S.A.; Mura, J.C. 2008. Avaliação de Imagens Multipolarizadas de Radar (Banda L) do Sensor SAR-R99B para Mapeamento Geológico no Baixo Vale do Rio Curaçá, Bahia. *Brazilian Journal of Geosciences*, 38: 706-721.